Wideband infrared trap detector based upon doped silicon photocurrent devices

S.I. WOODS,[1,*], J.E. PROCTOR[2], T.M. JUNG[2], A.C. CARTER[2], J. NEIRA[2], D.R. DEFIBAUGH[1]

[1]*Sensor Science Division, National Institute of Standards and Technology, Gaithersburg, MD 20899, USA*
[2]*Jung Research and Development Corp., Bethesda, MD 20816 USA*
**Corresponding author: solomon.woods@nist.gov*

Received:

We have designed, fabricated and measured infrared trap detectors made from arsenic-doped silicon (Si:As) blocked impurity band (BIB) photodetectors. These trap detectors are composed of two detectors in a wedge geometry, with an entrance aperture diameter of either 1 mm or 3 mm. The detectors were calibrated for quantum efficiency against a pyroelectric reference detector using a Fourier transform spectral comparator system, and etalon effects and spatial uniformity of the traps were also quantified. Measurements of the traps at a temperature of 10 K show that nearly ideal external quantum efficiency (> 90 %) can be attained over much of the range from 4 µm to 24 µm, with significant responsivity from 2 µm to 30 µm. The traps exhibited maximum etalon oscillations of only 2 %, about 10 times smaller amplitude than those of the single Si:As BIB detectors measured under similar conditions. Spatial non-uniformity across the entrance apertures of the traps was about 1 %. The combination of high detectivity, wideband wavelength coverage, spectral flatness, and spatial uniformity make these trap detectors an excellent reference detector for spectrally-resolved measurements and radiometric calibrations over the near- to far-infrared wavelength range.

OCIS codes: *(040.3060) Detectors, infrared; (040.2235) Detectors, far infrared; (040.5150) Detectors, photoconductivity; (120.3940) Instrumentation, metrology; (120.5630) Instrumentation, radiometry; (300.6340) Spectroscopy, infrared*

DOI:

1. INTRODUCTION

Optical trap detectors composed of multiple planar semiconductor devices are an important tool for radiometric calibrations, but until now have been very limited in their infrared (IR) spectral coverage. Trap detectors were first developed using silicon photodiodes, and often serve as intercomparison reference standards in the visible and near-IR [1-4]. A few groups have also published results in the near-IR using traps made from InGaAs photodetectors [5,6]. Trap detectors can attain external quantum efficiency near 100 % and when made from devices with excellent characteristics (e.g., spatial uniformity, high detectivity, low dark current), the traps inherit those performance capabilities. In this work, we present results on a wideband infrared trap detector with responsivity from 2 µm to 30 µm and external quantum efficiency > 90 % for most of the range from 4 µm to 24 µm.

For our wideband infrared trap detector, we have used arsenic-doped silicon (Si:As) blocked impurity band (BIB) detectors. Although these detectors are not readily available commercially, they have been the detector of choice for mid- and far-IR calibrations by the National Institute of Standards and Technology (NIST) [7], and for Earth- and satellite-based mid-IR telescopes and imagers developed by the National Aeronautics and Space Administration (NASA) [8-10] from soon after their development in the 1980s [11]. The Si:As BIB detector is operated at a temperature near 10 K, and for typical arsenic doping levels its external quantum efficiency is greater than 10 % from 2 µm to 30 µm, with a maximum of about 60 % from 14 µm to 22 µm. Not only do these detectors exhibit wide IR responsivity, but they also have excellent spatial non-uniformity of about 1 % over square millimeters and low dark current of 10^{-10} A/mm^2 at 10 K. The dark current scales with an activated response, as shown in Figure 1, so that by 7 K it is near 10^{-12} A/mm^2.

Compared to other detector types with sensitivity in the longwave-IR, the Si:As BIB detector has significant advantages. The detectivity of these photodetectors can be as high as 10^{14} cm·Hz$^{1/2}$·W^{-1} [12]. Their maximum operating frequency, which depends on the time required for photo-generated holes to hop between neighboring As sites to the back contact, can reach 1 MHz. Compared to typical thermal detectors of similar size they are much more sensitive and have faster response: they are 10^3 times more sensitive and 10^2 times faster than cryogenic bolometers, and they are 10^5 times more sensitive and 10^3 times faster than room-temperature pyroelectric detectors. Compared to typical mercury cadmium telluride (MCT) detectors, Si:As BIB detectors are responsive out to longer wavelengths and are much more spatially uniform. In addition, the family of BIB detectors based upon doped Si, Ge, and GaAs, shows promise for further improvements to capabilities in far-infrared and terahertz sensing [13-15]

The BIB detector is a photoconductive device with IR sensitivity from a heavily-doped impurity band ($\sim 1\times10^{18}$ cm^{-3} dopant concentration), and maintains low dark current with an undoped silicon blocking layer between its electrodes. Figure 2 provides a schematic for a backside-illuminated Si:As BIB device to illustrate photodetection and the mechanism of the blocking action. In a backside-illuminated detector, photons must pass through the detector substrate before reaching the sensing layer, the Si:As IR active layer (IRAL). Transparent contacts around the IRAL are used to bias the device, and are usually made from degenerately-doped Si:As. The aluminum front layer reflects any signal which is transmitted entirely through the device. In a single detector, this layer boosts detector external quantum efficiency by passing the beam twice through the IRAL before leaving the device. External quantum efficiency (EQE) is the ratio of signal registered by the detector to the total signal, and the internal quantum efficiency (IQE) is the ratio of signal registered by the detector to the total signal absorbed by the detector. In the trap detector, this reflective layer is also essential to capturing the non-absorbed signal after each bounce, and limiting light which escapes from the trap. For the wavelength range 2 μm to 30 μm, the reflectance of thin film aluminum can be greater than 98 % [16]. The positive charge carriers are the ionized As$^+$ ions, which are at high enough density that they are effectively mobile through the action of electron hopping between As donor sites. There are also always some acceptor impurity sites, which are not mobile due to their very low concentration.

The BIB detector works as intended only when biased in the polarity shown in Figure 2b, with the front contact near the blocking layer at the higher voltage. In the absence of photons, device current is minimized by the blocking layer and by carrier depletion in the IR-active layer. The positive As$^+$ ions must diffuse from the front to back contacts, but they cannot be supplied from the front contact due to the intervening blocking layer, which contains no As donor sites: this is the mechanism by which donor ion current is suppressed. Charge separation in the IRAL occurs because the mobile As$^+$ ions move toward the back contact and cannot be replenished, but the negative acceptor ions (often boron) are not mobile and are left behind. This depleted region will have few As+ ions and negative overall space charge which will impede the flow of electrons from the back contact: this is the mechanism by which electron current is suppressed.

With light incident on the device, a photon can be absorbed in the depleted region at a donor site, releasing a positive donor ion and a conduction electron. The As$^+$ ions move toward collection at the back contact and electrons are swept to the front contact. Collection efficiency of electrons is high because there is very low concentration of As$^+$ ions in the depleted region. For low light levels, the concentration of photo-generated electrons is also low, so collection efficiency of donor ions can also be very high. If the photons pass through a relatively thick (> 100 μm) Si substrate before reaching the IRAL, absorption in the silicon will be the primary source of internal loss. For a well-chosen bias voltage, about 2 V in typical devices, the detection efficiency and the gain of the IRAL can be near unity. If the bias voltage is too low, the width of the fully depleted region will be very small and quantum efficiency of the IRAL will fall, whereas if it is too high, impact ionization at the back contact will generate additional electrons and raise the gain above unity.

For many cryogenic experiments the Si:As BIB detector has unique capabilities for wideband infrared measurements, but for spectral measurements it has an inherent weakness due to its thin film construction. Etalon, or channeling, effects can be quite pronounced for BIB detectors, with oscillations in the spectral response due to coherent interference of light reflected between the top and bottom layer of the IRAL, and between the top and bottom of the entire device. Figure 3 shows the spectral response of a single BIB device from 750 cm^{-1} to 1050 cm^{-1} (13.3 μm to 9.5 μm) showing oscillations as large as 10 %, and two different oscillation periods. The oscillation with 4 cm^{-1} period is from interference across the silicon substrate (width 350 μm) and the larger 72 cm^{-1} period is from interference across the IRAL (width 15 μm). The oscillation periods expected from a simple estimate, $\Delta\sigma = \dfrac{1}{2nw\cos\theta}$ (index of refraction n, layer width w, angle of incidence θ), are 4.2 cm^{-1} and 98 cm^{-1}, in reasonable agreement with the results. The long period oscillation in the transmittance of the non-biased device is 95 cm^{-1} [17], but this period is reduced in the measurement of photo-response in the biased device. In terms of wavelength, the oscillation period is $\Delta\lambda = \lambda^2 d\sigma$, so at 10 μm the oscillation periods are approximately 0.04 μm and 1 μm. Low uncertainty narrowband spectral measurements and radiometry with the BIB detector are thus problematic, if the response can change by nearly 10 % when the wavelength changes by only 40 nm.

Development of a trap detector using Si:As BIB photodetectors has two distinct motivations. The first is that it provides, over a wide range of the IR, the standard capabilities of a trap detector which are valued for radiometry: near ideal response (i.e., unity EQE) and no back-reflection. The second motivation is that the trap arrangement can wash-out the prominent etalon effect of BIB detectors and secure all the excellent qualities of Si:As BIB photodetectors in a device which can be used for low uncertainty measurements over well-defined spectral limits. Etalon oscillations are a result of spatial phase coherence, but in a trap where the angle of incidence is different on each bounce, the phase is effectively randomized.

2. DESIGN OF THE TRAP

We employed a wedge geometry for the light-trapping detector composed of two Si:As BIB detectors (BIB trap). By using only two detectors, the dark current is kept small, and as light bounces down the wedge, the angle of incidence at each detector changes. The critical parameters defining the wedge trap are the initial angle of incidence and the angle between the detectors in the wedge (see Figure 4). We modeled the behavior of such a wedge to determine the values of these two parameters which would minimize the area of detectors required to capture all the light, given a fixed aperture size at the entrance of the trap. Smaller detectors will exhibit less noise and also lead to a more compact design. Starting with an $f/4$ beam focused at the aperture of the trap, we considered how the

beam area would increase for a wedge with a minimum of 7 bounces before escape from the trap.

Results of the modeling identified the optimal initial angle of incidence and the optimal wedge angle to be 49 degrees and 14 degrees, respectively. Figure 5a shows how the detector area scales with initial angle of incidence and wedge angle, for the case of a 3 mm diameter entrance aperture. Although smaller areas are possible for very small wedge angles, for ease of construction we settled on 14 degrees for the minimum wedge angle to use. For a 3 mm diameter entrance aperture and a fixed wedge angle of 14 degrees, Figure 5b shows how detector area depends upon initial angle of incidence, identifying 49 degrees as the initial angle which yields the minimum area. Based on the modeling, we determined that for a 3 mm diameter aperture and an incoming beam with $f/4$ divergence, it would be possible to employ a rectangular detector with active area dimensions of approximately 7.4 mm x 9.7 mm.

The mechanical assembly for the BIB trap is shown in Figure 6. The rigid mount is made from Invar to minimize thermal contraction during cooldown, and differential contraction between Invar and silicon is very small. Gold-plating is used to minimize oxidation of the Invar when in ambient conditions. For modularity, the detectors are epoxied into silicon carriers, and these carriers are epoxied to the mount. In this way the detectors can be positioned and wire-bonded on the carriers before being attached to the mount. A small circuit board, with coaxial connectors, is attached to one face of the trap for the bias, signal and guard connections to the detectors. The detectors share the same bias and guard, and their signal lines are summed for a single output. A polyimide flex circuit with copper traces connects the detectors to the circuit board. An aperture well at the top of the mount can accept a precision aperture.

3. EXPERIMENTAL PROCEDURE

All measurements were made using a spectral detector comparator system based around a Fourier transform spectrometer (FTS), using the FTS as the light source and comparing response of the BIB detectors to that of a calibrated pyroelectric detector [18]. The schematic in Figure 7 shows the layout of this instrument. Nearly collimated light from the FTS first passes through a spatial filter with a 150 μm aperture, and is directed to an off-axis gold-coated parabolic mirror mounted on top of 3 mechanical stages. One of the stages is a rotation stage which can direct the beam to the left in the figure (the pyroelectric reference detector) or to the right (the BIB trap detector under test). One linear stage can focus the beam at the detector being measured. Another linear stage and the rotation stage are used to scan the beam over the detectors for spatial uniformity measurements. Spatial uniformity was measured as a function of wavelength by operating the FTS normally. It was also possible to measure broadband spatial uniformity by stopping the spectrometer's internal scanning mirror and measuring the chopped blackbody signal from the globar source of the spectrometer. A purge box, supplied with air filtered of CO_2 and H_2O, covers all the measurement components between the FTS and the detector under test, to reduce atmospheric absorptions in the infrared.

Automated software control was used to execute EQE measurements, with the beam sequentially moved between reference and test detectors. Each measurement cycle consisted of data collection at each detector, so the test detector response could be scaled by the reference, and a cycle lasted no more than 30 minutes, in order to minimize drift. Multiple cycles were collected over up to 12 hours and then averaged. Etalon measurements were made at high FTS spectral resolution (~ 1 cm^{-1}) and all other measurements were typically made at 32 cm^{-1} resolution. The uncertainty (k =2) of the calibration on the pyroelectric reference detector was approximately 0.024 V/V (2.4 %) from 1.6 μm to 19 μm and 0.050 V/V (5.0 %) above 19 μm. All measurements were made with the BIB detectors at a temperature of 10 K, temperature-controlled with stability of 0.1 mK.

4. RESULTS AND DISCUSSION

A. Single BIB Detectors

We measured two different types of Si:As BIB detectors, and assembled trap detectors based on each of them. The first type of detector (denoted Type 1) is backside-illuminated with a relatively thick substrate (350 μm) and relatively thin IRAL (15 μm). Type 1 detectors have a maximum area of approximately 3 mm x 3 mm. The second type of detector (denoted Type 2) is also backside-illuminated, with the substrate polished away, and a relatively thick IRAL (54 μm). Type 2 detectors were made in three sizes, with the maximum detector area of 11.5 mm x 15 mm sufficient for a trap design with a 5 mm diameter circular aperture. Type 1 detectors exhibited excellent spectral responsivity, near optimal for Si:As BIB detectors, and the trap made from these detectors had the best EQE. Although the spectral responsivity of the Type 2 detectors was relatively poor, due to fabrication problems, it was possible to fabricate larger aperture traps from these larger detectors. Performance results such as spectral flatness and spatial uniformity were more completely tested using these larger traps.

Quantum efficiency data for the single Type 1 detectors has been published before [19] and is reproduced in Figure 8. These detectors are operated at a reverse bias of 2 V and exhibit a maximum efficiency near 60 %. The EQE is calculated by dividing the responsivity (in A/W) by the ideal response (λe/hc) for a photon-counting detector. The structures evident in the FTS data near 9 μm and 16 μm are from the most significant absorptions in silicon, and these noticeable features are due to the relatively thick substrate. Quantum efficiency data for the single Type 2 detectors in Figure 8 show that these detectors are significantly poorer for wavelengths beyond 10 μm. The arsenic doping of these detectors was measured by secondary ion mass spectrometry (SIMS) after fabrication and found to be 60 % to 90 % higher than the target of 1×10^{-18} cm^{-3}. At such high doping (weakly degenerate), it is difficult to maintain depletion in the IRAL, and so dark current and recombination are elevated. These detectors were operated at a reverse bias of 6 V to improve depletion, but higher biases result in elevated gain at shorter wavelengths due to impact ionization. A positive attribute of these detectors is that the silicon absorptions seen in Type 1 detectors are absent because Type 2 detectors have no silicon substrate layer.

The magnitude of the etalon oscillations are similar for Type 1 and Type 2 detectors, but the period of oscillations differ due to the different layer thicknesses in the two devices. In particular, the total thickness for the Type 2 detectors is about 6 times less than for the Type 1 detectors, so the shorter period is about 25 cm^{-1} rather than 4 cm^{-1}. Figure 9 shows the spectral structure from 1980 cm^{-1} to 2180 cm^{-1} (5.1 μm to 4.6 μm) for a Type 2 detector. This spectral range shows oscillations of approximately 17 % full depth. The depth varies with wavenumber (wavelength), is a maximum of 24 % near 2600 cm^{-1} (3.8 μm), and falls off at lower wavenumbers to about 5 % at 1100 cm^{-1} (9.1 μm). The depth of the etalon oscillations depends upon the complex index of refraction of the Si and IRAL, which have significant spectral character.

In earlier work, we used reflectance and transmittance measurements to determine the complex index of refraction of the IRAL in the Type 1 detectors [17]. A simple analysis, ignoring coherence effects, derived the spectral curves for n_{IRAL} and k_{IRAL} of the

Si:As IR active layer, shown in Figure 10. With these extracted values it is possible to calculate the total reflectance (R_{tot}) from a Type 1 detector, assuming no internal losses in the IRAL. Over the range from 10 μm to 23 μm, the value of the EQE measured agrees with "$1 - R_{tot}$" to within 15 %, indicating that internal losses and transmission are not large. Of the total signal reflected from the detector, about 30 % is reflected at the incident silicon substrate surface; 10 % passes through the detector, bounces off the aluminum top layer, passes through the detector a second time and then exits back out the silicon substrate. From the k_{IRAL} curve in Figure 10, it can be seen that absorption in the detectors is low at short wavelengths and increases with increasing wavelength. Low EQE below 10 μm is caused by low absorption, whereas low EQE above 23 μm is a result of low IQE. In the Type 2 detectors, the IRAL is more than 3 times thicker, so absorption in the devices is expected to be higher than in the Type 1 detectors. Despite this, the EQE is significantly lower, implying that internal losses are large for Type 2 detectors.

Spatial uniformity data for Type 1 Si:As BIB detectors has been measured [20] and indicated non-uniformity of about 1 % over an area of 2 mm x 2mm. Results on Type 2 detectors are similar and are shown in Figure 11. Spatial uniformity was measured by scanning the output of the FTS over the face of the detector, and recording the response at a fixed wavelength. The non-uniformity in the plateau region of the linescan is 1.4 % full range, and the standard deviation in response over the plateau region is about 0.69 %.

B. BIB traps

External quantum efficiency for a Type 1 BIB trap with a 1 mm aperture is shown in Figure 12a. The EQE is nearly ideal over much of the range from 4 μm to 24 μm and there is significant responsivity from 2 μm to 30 μm. The error bars, shown at 4 selected wavelengths, result partly from uncertainty (calibration and noise) associated with the calibrated reference pyroelectric detector used for calibrating the BIB trap responsivity. The pyroelectric detector carries a 2.4 % to 5.0 % uncertainty (k =2) in its calibration over the measured range, and it is much less sensitive than the BIB trap, so its noise level (about 0.4 % to 2 %, depending on wavelength) is much higher for similar integration times. There is additional uncertainty associated with the transmission of a window and filter in the cryostat. Figure 12b shows the EQE for a Type 2 BIB trap with a 3 mm aperture. The EQE is significantly improved from the EQE for a single Type 2 BIB detector but is still far from ideal. However, there are only weak absorption features in the EQE, in contrast to the Type 1 case. Analysis of the Type 2 single detector and trap results indicates that nearly all the light transmitted past the incident surface of each detector is absorbed, but that internal losses are high.

Compared to the single detectors, the depth of etalon oscillations in Type 1 and Type 2 BIB traps is about 10 times smaller. Figure 13 shows that the full depth of oscillations is about 2 % in contrast to the up to 20 % depth exhibited for the Type 2 single BIB detector. FTS scans at different wavenumber resolutions were made to ensure that etalon oscillation depth was fully resolved, by increasing resolution until oscillation depth saturated. Type 2 BIB traps, even though they do not have ideal EQE, can be used for low-uncertainty IR spectral calibrations because the effects of phase coherence have been much reduced.

The spatial non-uniformity of the Type 1 and Type 2 BIB traps across their entrance aperture is approximately 1 %, inherited from the excellent spatial uniformity of the single detectors. Figure 14a shows a linescan across the 1 mm diameter entrance aperture of the Type 1 BIB trap. The beam spot size is approximately 600 μm diameter so the plateau region is limited to about 400 μm diameter, but over this region the maximum variation in response is 1.1 %, and the standard deviation over the plateau is 0.43 %. Figure 14b shows a scan of the 3 mm diameter entrance aperture of a Type 2 BIB trap, where the maximum variation over the plateau region is 0.46 %, and the standard deviation over the plateau is 0.14 %. The Type 2 results better represent the spatial uniformity of the trap responsivity because the small Type 1 aperture severely limits the plateau region and introduces significant diffraction effects at longer wavelengths.

5. CONCLUSIONS

We have designed, fabricated, and measured infrared trap detectors made from two types of Si:As BIB photodetectors. These BIB traps boost the quantum efficiency attainable with BIB detectors, reduce unwanted etalon effects by a factor of 10, and exhibit excellent spatial non-uniformity near 1 %. A trap made from the Type 1 detectors has EQE near unity over much of the range from 4 μm to 24 μm. Given the relatively smooth spectral response and minimal back reflection of both Type 1 and Type 2 BIB traps, these detectors are well-suited for broadband and spectrally resolved measurements from 2 μm to 30 μm. The BIB trap is an attractive reference detector which can be used to transfer optical power scales in the infrared. For instance, it can be used in rapid scan FTS measurements to spectrally calibrate infrared sources in units of power, and it can be used for comparing primary standards at important infrared laser wavelengths such as 10.6 μm.

Further tests and development could improve the applicability of BIB traps. Low uncertainty calibrations at IR laser wavelengths will reduce the error in the EQE determination of the trap at discrete wavelengths. Tests of power linearity, particularly at low powers, will help quantify the range of optical power over which these detectors can transfer and maintain optical power scales. All experiments reported here used room-temperature current amplifiers for detector readout, but coupling a trap detector with a cryo-amplifier in a low-background environment would significantly improve the noise performance of the detectors [21]. Development of applications for BIB detectors is severely hampered by limited availability of these detectors. The fabrication of larger (≥ 5 mm x 5mm) high EQE BIB detectors would enable a BIB trap with larger aperture (≥ 3 mm) and unity EQE over much of the near- to far-IR wavelengths.

Acknowledgements. The authors would like to thank Vyacheslav Podobedov (NIST) for calibration of the pyroelectric detector used in the study and David Simons (NIST) for making SIMS measurements on the Type 2 BIB detectors.

References

1. E.F. Zalewski and C.R. Duda. *Silicon photodiode device with 100 % external quantum efficiency*. Applied Optics **22** (18) 2867 (1983).
2. S. G. R. Salim, K. Anhalt, D. R. Taubert, and J. Hollandt. *Three-element trap filter radiometer based on large active area silicon photodiodes*. Applied Optics **55** (15) 3958 (2016).
3. M. Sildoja, F. Manoocheri and E. Ikonen. *Reflectance calculations for a predictable quantum efficient detector*. Metrologia **46** S151 (2009).
4. J.Y. Cheung, C.J. Chunnilall, G. Porrovecchio, M. Smid, and E. Theocharous. *Low optical power reference detector implemented in the validation of two independent techniques for calibrating photon-counting detectors*. Optics Express **19** (21) 20347 (2011).
5. Vaigu, T. Kübarsepp, F. Manoocheri, M. Merimaa, and E. Ikonen. *Compact two-element transmission trap detector for 1550 nm*

wavelength. Measurement Science and Technology **26** 055901 (2015).
6. K. D. Stock and R. Heine. *Spectral characterization of InGaAs trap detectors and photodiodes used as transfer standards*. Metrologia **37** 449 (2000).
7. T.M. Jung, A. C. Carter, S.I. Woods, and S.G. Kaplan. *Calibration and Deployment of a New NIST Transfer Radiometer for Broadband and Spectral Calibration of Space Chambers (MDXR)*. Technologies for Synthetic Environments: Hardware-in-the-Loop XVI (eds. Scott B. Mobley and R. Lee Murrer, Jr.). Proc. of SPIE **8015** 80150C-1 (2001).
8. G.H. Rieke, M.E. Ressler, J.E. Morrison, L. Bergeron, P. Bouchet, M. Garcia-Marin, T.P. Greene, M.W. Regan, K.G. Sukhatme, and H. Walker. *The Mid-Infrared Instrument for the James Webb Space Telescope, VII: The MIRI Detectors*. Publications of the Astronomical Society of the Pacific **127** 665 (2015).
9. A.K. Mainzer, H. Hogue, M. Stapelbroek, D. Molyneux, J. Hong, M. Werner, M. Ressler, E. Young. *Characterization of a megapixel mid-infrared array for high background applications*. High Energy, Optical and Infrared Detectors for Astronomy III (eds. David A. Dorn and Andrew D. Holland). Proc. of SPIE **7021**, 70210T (2008).
10. L.D. Keller, T. Hertera, G. Stacey, G. Gu1, J. Schoenwalda, B. Pirgera, J. Adamsa, M.G. Berthoud, T. Nikola. *First test results from FORCAST: the facility mid-IR camera for SOFIA.* Ground-based Instrumentation for Astronomy (eds. Alan F. M. Moorwood and Masanori Iye). Proc. of SPIE **5492** 1086 (2004).
11. M.D. Petroff and M.G. Stapelbroek. *Responsivity and noise models of blocked impurity band detectors*. IRIA-IRIS, Proceedings of the Meeting of the Specialty Group on Infrared Detectors (Seattle, August 1984) Volume II. ERIM (Ann Arbor, Michigan), 1984.
12. F. Szmulowicz, F.L. Madarsz and J. Diller. *Temperature dependence for the figures of merit for blocked impurity band detectors*. J. Appl. Phys. **63** (11) 5583 (1988).
13. X. Wang, B. Wang, Y. Chen, L. Hou, W. Xie, X. Chen, and M. Pan. *Spectral response characteristics of novel ion-implanted planar GaAs blocked-impurity-band detectors in the terahertz domain*. Optical and Quantum Electronics **48** (518) 1 (2016).
14. M. Hanaoka, H. Kaneda, S. Oyabu, M. Yamagishi, Y. Hattori, S. Ukai, K. Shichi, T. Wada, T. Suzuki, K. Watanabe, K. Nagase, S. Baba, and C. Kochi. *Development of Blocked-Impurity-Band-Type Ge Detectors Fabricated with the Surface-Activated Wafer Bonding Method for Far-Infrared Astronomy*. Journal of Low Temperature Physics **184** 225 (2016).
15. K.S. Liao, N. Li, C. Wang, L. Li, Y.L. Jing, J. Wen, M.Y. Li, H. Wang, X.H. Zhou, Z.F. Li, and W. Lu. *Extended mode in blocked impurity band detectors for terahertz radiation detection*. Applied Physics Letters **105**, 143501 (2014).
16. D.Y. Smith, E. Shiles, and M. Inokuti. *The Optical Properties of Metallic Aluminum*, in Handbook of Optical Constants of Solids (ed. Edward D. Palik). Academic Press, Inc. (Orlando), pp. 369-406, 1985.
17. S.I. Woods, S.G. Kaplan, T.M. Jung, and A.C. Carter. *Characterization of the optical properties of an infrared blocked impurity band detector*. Applied Optics **50** (24) 4824 (2011).
18. V.B. Podobedov, G.P. Eppeldauer, T.C. Larason. *Evaluation of optical radiation detectors in the range from 0.8 µm to 20 µm at the NIST infrared spectral calibration facility*. Optical Systems (ed. by Pablo Benítez, et al.). Proc. of SPIE **8550**, 855029 (2012).
19. A.C. Carter, S.R. Lorentz, T.M. Jung, B. J. Klemme and R.U. Datla. *NIST Facility for spectral calibration of detectors: calibration of arsenic doped silicon blocked impurity band detectors*. Infrared Detectors and Focal Plane Arrays VI (eds. Eustace L. Dereniak and Robert E. Sampson). Proc. of SPIE **4028** 420 (2000).
20. E.J. Iglesias, A.W. Smith and S.G. Kaplan. *A sensitive, spatially uniform photodetector for broadband infrared spectrophotometry*. Applied Optics **47** (13) 2430 (2008).
21. J.E. Proctor, A.W. Smith, T.M. Jung, and S.I. Woods. *High-gain cryogenic amplifier assembly employing a commercial CMOS operational amplifier*. Review of Scientific Instruments **86**, 073102 (2015).

Figures

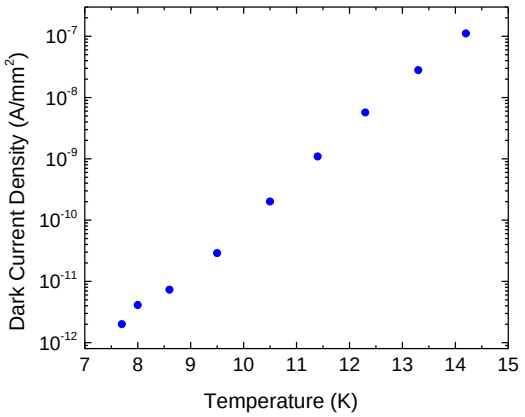

Fig. 1. Dark current density for a Si:As BIB detector, showing activated response. At 10 K, the dark current density is about 0.1 nA/mm2 and by 7 K approaches 1 pA/mm2.

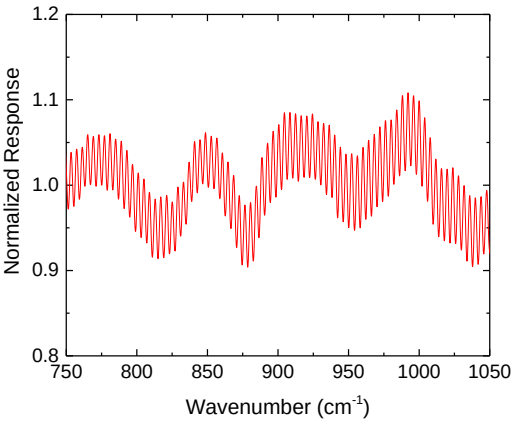

Fig. 3. Spectral response of a single Si:As BIB detector from 750 cm^{-1} to 1050 cm^{-1}, showing two different periods of etalon oscillation, and full oscillation amplitude as large as 10 %.

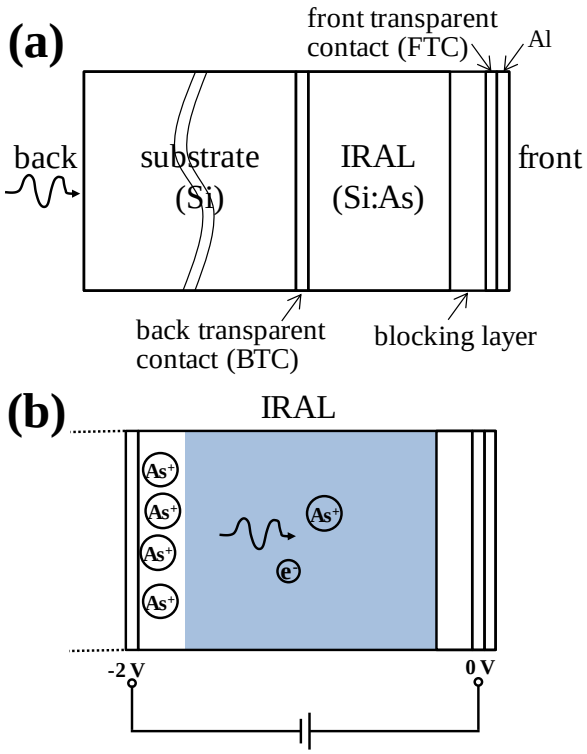

Fig. 2. (a) Schematic of a backside-illuminated BIB detector, where the incident light passes through the silicon substrate before reaching the IR active layer; (b) diagram showing voltage and charge configuration around the IRAL of the Si:As BIB detector. The detector must be biased in the polarity shown for low noise performance, and the shaded region contains negative space charge from immobile acceptor ions.

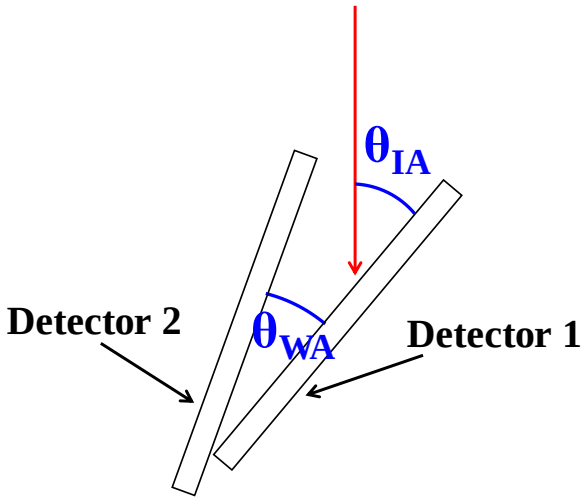

Fig. 4. Schematic of the 2-detector wedge trap design, with the red arrow indicating the incident light. The two critical design parameters, the initial angle of incidence (θ_{IA}) and the wedge angle (θ_{WA}), are indicated.

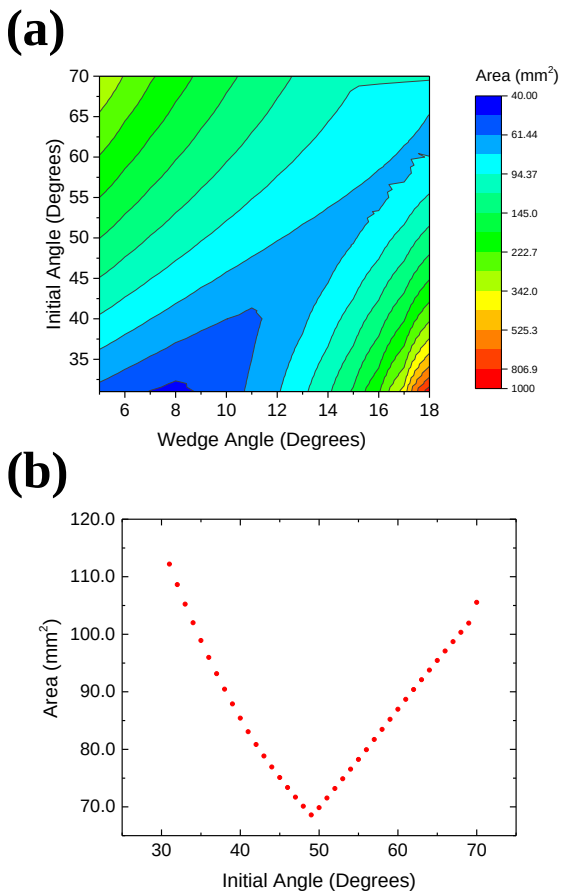

Fig. 5. (a) Modeling results for the detector area as a function of the initial angle of incidence and the wedge angle; (b) Modeling results for the detector area as a function of initial angle of incidence, with the wedge angle fixed at the selected value of 14 degrees.

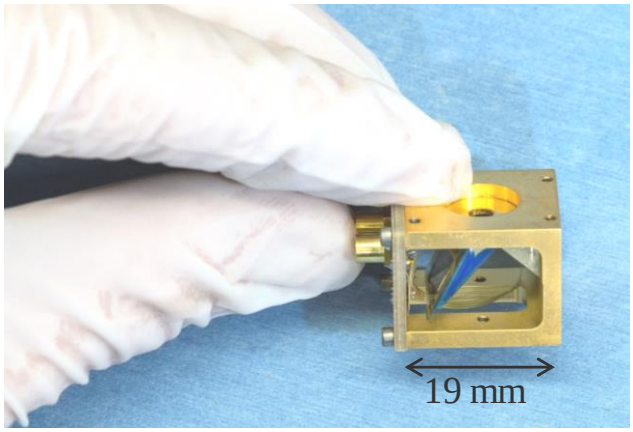

Fig. 6. Photograph of the BIB trap detector, held by a gloved hand for scale. The detectors are mounted on either side of the blue wedge in the middle of the assembly; the flex circuits attached to the detectors, the aperture well at top, and the connectorized circuit board on the left are visible.

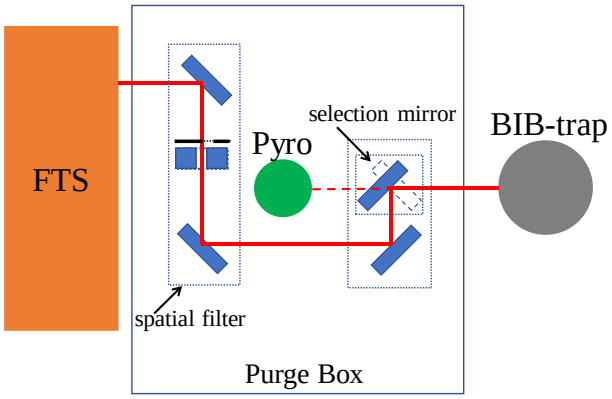

Fig. 7. Schematic of the experimental system used to make FTS-based spectral measurements of the BIB detectors. Capabilities include spectral calibration against a reference pyroelectric detector, high resolution spectral responsivity, and spatial uniformity of detector responsivity in the spectral range from 1 μm to 40 μm.

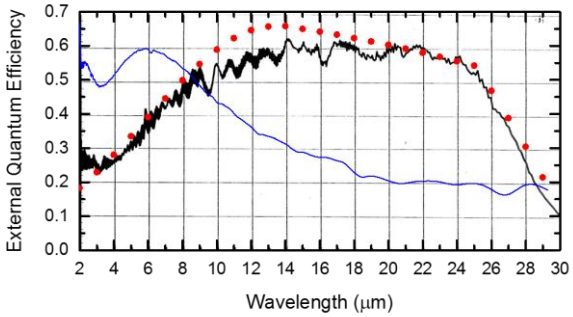

Fig. 8. External quantum efficiency as a function of wavelength for Type 1 and Type 2 Si:As single BIB detectors. The black line shows FTS data from the manufacturer for a Type 1 detector, the red dots show monochromator data published earlier [19] for a Type 1 detector, and the blue line shows FTS data for a Type 2 detector measured in this study.

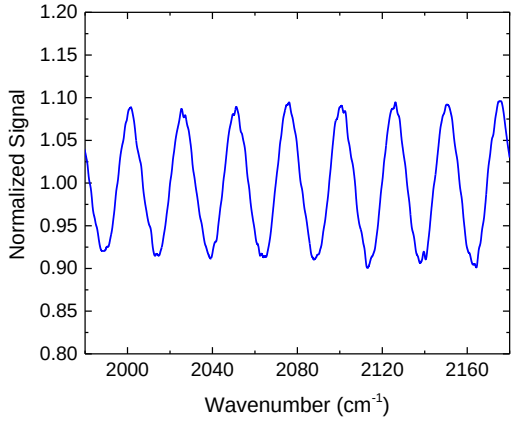

Fig. 9. Etalon oscillations from 1980 cm^{-1} to 2180 cm^{-1} for a Type 2 single BIB, exhibiting a full oscillation amplitude of 17 % and a period of 25 cm^{-1}.

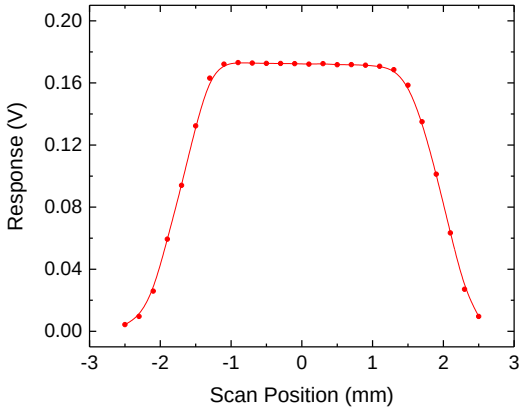

Fig. 11. Response linescan across a Type 2 single BIB detector, showing a full range non-uniformity of 1.4 % over the plateau region. The standard deviation over the plateau region is 0.69 %.

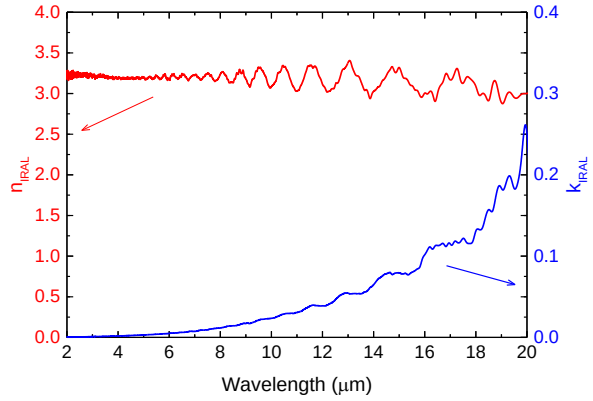

Fig. 10. Complex index of refraction data for the IRAL in the Type 1 BIB detectors published earlier [17]. The value of k_{IRAL} increases significantly as wavelength increases, and n_{IRAL} drifts down slightly as wavelength increases. At short wavelengths, a significant amount of light can make two passes through the IRAL without being absorbed.

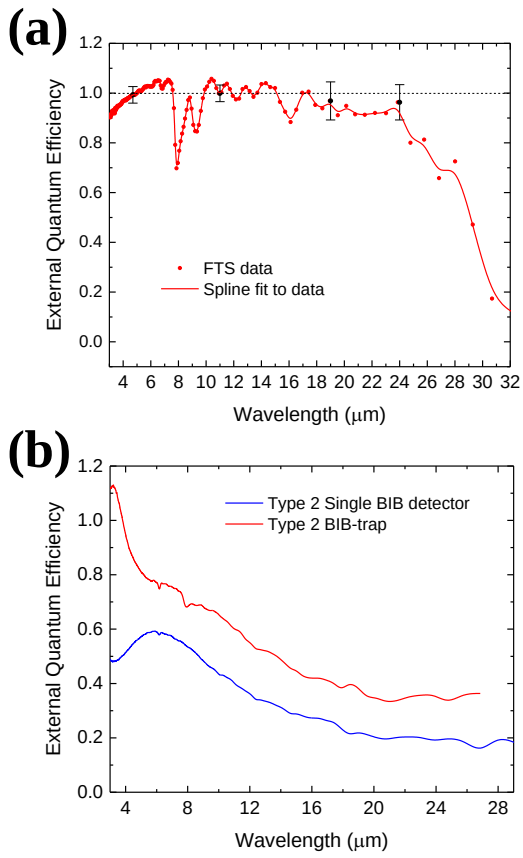

Fig. 12. (a) External quantum efficiency of a Type 1 BIB trap, showing nearly ideal response (EQE > 90 %) over most of the range from 4 μm to 24 μm. Error bars (k=2 uncertainty) are shown at 4 wavelengths; (b) External quantum efficiency of a Type 2 BIB trap, compared to a Type 2 single BIB detector. Although the trap exhibits higher EQE, its response is still far from ideal over most of the range.

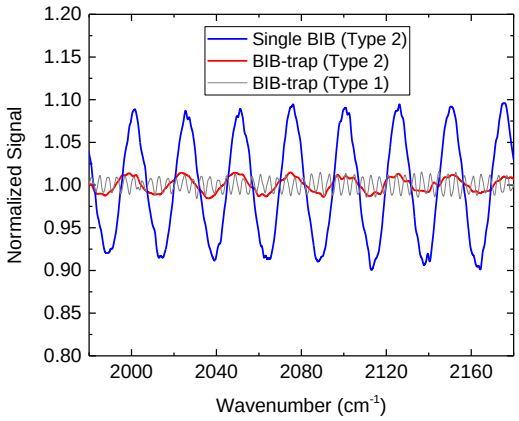

Fig. 13. Comparison of etalon oscillations in a single BIB detector and BIB traps. The full depth of oscillations in the BIB traps is only about 2 %.

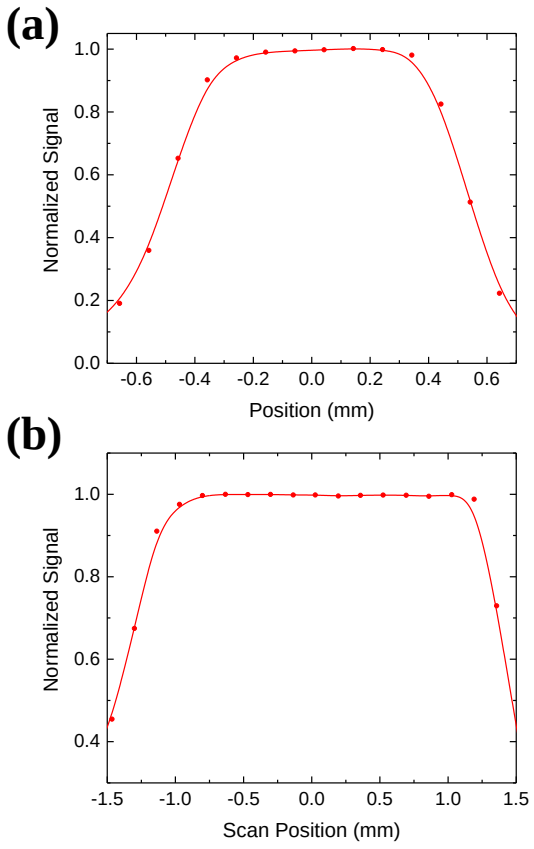

Fig. 14. (a) Response linescan across a Type 1 BIB trap (with 1 mm diameter aperture), exhibiting a plateau region with 1.13 % full range non-uniformity and 0.43 % standard deviation; (b) Response linescan across a Type 2 BIB trap (with 3 mm diameter aperture), exhibiting a plateau region with 0.43 % full range non-uniformity and 0.14 % standard deviation.